


## Flexible gas sensor based on rGO-ZnO for NO<sub>2</sub> detection at room temperature

Amanda Akemy Komorizono<sup>a,b,\*</sup> , Ramon Resende Leite<sup>a</sup>, Silvia De la Flor<sup>c</sup>, Eduard Llobet<sup>b</sup>, Valmor Roberto Mastelaro<sup>a</sup>

<sup>a</sup> Institute of Physics of São Carlos, University of São Paulo, 13566-590, São Carlos, SP, Brazil

<sup>b</sup> Universitat Rovira i Virgili, MINOS, Avda. Països Catalans, 26, 43007, Tarragona, Spain

<sup>c</sup> Department of Mechanical Engineering, Universitat Rovira i Virgili, Avda. Països Catalans, 26, 43007, Tarragona, Spain

### ARTICLE INFO

#### Keywords:

Flexible gas sensor  
NO<sub>2</sub> sensor  
rGO-ZnO gas sensor  
PET substrate

### ABSTRACT

In recent decades, there has been extensive research into sensors for detecting toxic gases and volatile organic compounds (VOCs). However, creating a gas sensor that combines high sensitivity, selectivity, and stability at room temperature (RT) remains challenging. Additionally, there is a growing need for flexible gas sensors that can monitor environmental conditions in real-time, suitable for use in accessories like bracelets and watches or even integrated into clothing. This study focuses on developing a flexible rGO-ZnO-based gas sensor deposited on a polyethylene terephthalate (PET) substrate for detecting NO<sub>2</sub> at room temperature using a fast, simple, and cost-effective methodology. Scanning Electron Microscopy (SEM) images reveal that the rGO-ZnO sensor consists of rGO sheets adorned with ZnO nanoparticles. Measurements show that the formation of rGO-ZnO heterostructures significantly enhances the sensor's response to NO<sub>2</sub> at RT compared to pure ZnO. The rGO provides a conductive pathway for efficient charge transport, while ZnO increases the number of active sites available for NO<sub>2</sub> molecule adsorption, leading to improved sensor performance. Moreover, the rGO-ZnO sensor exhibits high selectivity for NO<sub>2</sub> compared to other tested gases and demonstrates minimal change in response even after multiple bending cycles. In conclusion, our findings suggest that the rGO-ZnO flexible sensor offers excellent response, stability, flexibility, and selectivity, highlighting its potential for integration into clothing and accessories for real-time NO<sub>2</sub> monitoring at room temperature.

### 1. Introduction

Nitrogen dioxide (NO<sub>2</sub>), one of the most harmful gases present in air pollution gases, is a reddish-brown oxidizing gas, highly reactive, non-flammable, and with an irritating odor [1,2]. It is formed from the combustion of fossil fuels in power plants and vehicle engines and contributes to the formation of tropospheric ozone, acid rain, and global warming [3]. When humans are exposed to a concentration above the safety limit, the gas can harm the respiratory system and irritate the skin and eyes. NO<sub>2</sub> is widely used as a raw material in producing nitric acid, which is required for fertilizers and explosives in agriculture and industry. Because of its harmful effects on human health, the United States Environmental Protection Agency has established an environmental NO<sub>2</sub> concentration limit of 53 ppb for the annual average [4].

Technological advances have demanded the development of gas sensors with lower power consumption that are faster, more accurate,

versatile, low-cost, light, and small [5]. Flexible gas sensors have attracted significant interest from academia and the market in meeting those demands. The sensors can be integrated into watches, bracelets, glasses, clothes, and shoes, and they can even adhere to the skin of the human body to monitor environmental conditions in real-time [6,7].

Graphene has proven a promising candidate for gas sensing due to its excellent properties, such as high electron mobility at room temperature (RT) (~200,000 cm<sup>2</sup>/V.s), large surface area (~2630 m<sup>2</sup>/g), high thermal conductivity (~3000 W/m.K), high charge density (10<sup>12</sup> cm<sup>-2</sup>), and low resistivity (10<sup>-6</sup> Ω cm) [1]. Furthermore, it shows excellent mechanical flexibility and low operating temperature, making it an ideal candidate for fabricating flexible gas sensors [8]. Although gas sensors made from pristine graphene can detect gases at room temperature, the interaction between the surface of graphene and the target gases is weak, thus generating low response, long response times, and incomplete recovery [9]. Another factor influencing the low response of gas

\* Corresponding author. Institute of Physics of São Carlos, University of São Paulo, 13566-590, São Carlos, SP, Brazil.

E-mail address: [amanda.akemy@hotmail.com](mailto:amanda.akemy@hotmail.com) (A.A. Komorizono).

<https://doi.org/10.1016/j.mssp.2024.109229>

Received 11 November 2024; Received in revised form 9 December 2024; Accepted 16 December 2024

Available online 21 December 2024

1369-8001/© 2024 Elsevier Ltd. All rights reserved, including those for text and data mining, AI training, and similar technologies.

sensors based on pristine graphene is the absence of defects and functional groups. Furthermore, their relatively high production costs and low large-scale production capacity limit using pristine graphene for gas sensing [1]. In contrast, reduced graphene oxide (rGO), a graphene derivative obtained by the reduction of graphene oxide (GO), has defects and oxygenated functional groups and can be produced on a large scale and at a low cost [9]. However, rGO sensors still show low response, poor selectivity, and slow recovery due to their weak interaction with gases [10].

The formation of a heterostructure between rGO and metal oxide semiconductors (MOS) is a way to improve the material's sensing properties. MOS were the first materials investigated for toxic gas sensors and featured high sensitivity, high response, and low recovery times [11]. However, sensors based on pure MOS operate at high temperatures (>200 °C), which makes their use in flexible sensors unfeasible [10]. Studies have demonstrated that sensors based on rGO-MOS p-n heterostructure improve the sensitivity, selectivity, response, recovery times, and reduced temperature due to synergistic effects between the materials [8,12]. Among n-type MOS, zinc oxide (ZnO) is one of the most explored for the development of gas sensors. It has 3.37 eV bandgap, large exciton binding energy (60 meV), high electron mobility (200 cm<sup>2</sup>/V.s), and high chemical and thermal stability [7]. The heterostructures of rGO (p-type) with ZnO (n-type) have been widely explored due to their synergistic interactions [13].

In addition to the type of material used for detecting toxic gases, the choice of substrate is a crucial parameter. The substrate must be flexible, compatible with the sensor material in terms of adhesion, and withstand the conditions of gas detection measurements without degrading. Among the types of substrates used for manufacturing flexible sensors, we found paper, plastic, and fabric [7]. The plastic substrate is the most used among these substrates, especially for gas sensors. Plastic substrates are highly flexible and low-cost, and the substrates more explored for gas sensors are Polyethylene terephthalate (PET), Polyethylene naphthalate (PEN), Polyimide (PI), Polydimethylsiloxane (PDMS), and nylon [7,14]. The choice of which plastic will be used depends on the mechanical, electrical, and thermal properties to which the sensors will be exposed. Among plastic substrates, PET is an excellent candidate for flexible gas sensors at RT because is transparent, exhibits high flexibility, and is cheap. In terms of operating temperature, PET cannot be used at temperatures above 150 °C, which does not affect the choice of PET as a substrate since most flexible sensors operate at RT [14].

Su et al. (2014) reported a layer-by-layer fabricated rGO sensor on a PET substrate. This sensor showed a response of 11.5 % to 5 ppm NO<sub>2</sub> [15]. Yaqoob et al. (2016) developed a WO<sub>3</sub> NPS-based sensor decorated with MWCNTs-rGO on a PI/PET substrate for NO<sub>2</sub> detection at RT. This sensor exhibited a maximum response of 17 % to 5 ppm NO<sub>2</sub>, low response-recovery times (7/15 min), and high selectivity for NO<sub>2</sub> [16]. Kim et al. (2018) developed a MoS<sub>2</sub>-SWCNT sensor on a PET substrate, which exhibited a response of 54 % to 40 ppm NO<sub>2</sub> at RT [17]. Tian et al. (2022) fabricated a N-doped SWCNT sensor for NO<sub>2</sub> detection at 90 °C, which showed a response of 27.7 % to 10 ppm NO<sub>2</sub> and a recovery time of 53 min [18].

Over the past decade, numerous gas sensors based on rGO-ZnO have been documented in the literature [3,9,10,19–22]. However, most of these sensors operate at elevated temperatures (>100 °C), which increase costs, shorten their lifespan, and hamper their adoption in flexible wearables. Additionally, these studies typically focus on detecting high concentrations of NO<sub>2</sub>. Recently, some researchers have reported that rGO-ZnO sensors work at room temperature [23–26], but these devices are generally not flexible and cannot be integrated into clothing or accessories for real-time air monitoring. Consequently, there is still a significant gap in developing and investigating flexible rGO-ZnO-based gas sensors for NO<sub>2</sub> detection at room temperature, particularly regarding their sensing and mechanical properties.

In this study, we created a flexible heterostructured PET sensor utilizing rGO-5% ZnO, which has a detection limit of 1.5 ppm and exhibits

strong selectivity for NO<sub>2</sub> at room temperature. Our sensor is also cost-effective, as the ZnO nanoparticles were synthesized using a polymer precursor method that does not require sophisticated equipment or high temperatures. Additionally, the rGO-5% ZnO sensor maintains excellent flexibility, with minimal changes in response after numerous bending cycles.

## 2. Experimental section

### 2.1. Synthesis of ZnO

ZnO NPs were synthesized by the Pechini Method [27] with a ratio of 40:60 per mass of citric acid: ethylene glycol and a ratio of 3:1 by mole of citric acid: precursor. The precursor was zinc nitrate hexahydrate [Zn(NO<sub>3</sub>)<sub>2</sub>·6H<sub>2</sub>O]. Citric acid was dispersed in Milli-Q water under stirring and, when the solution became limpid, [Zn(NO<sub>3</sub>)<sub>2</sub>·6H<sub>2</sub>O] was added and the solution was heated. Ethylene glycol was added at 80 °C, and the solution was heated at 120 °C for 1 h. The final solution was transferred to a glass container and placed in an oven for 2 h at 300 °C at 10 °C/min rate to form a spongy structure called “puff”. In this heat treatment step, a brown powder containing organic materials was obtained, macerated, and treated again for 2 h at 500 °C at 10 °C/min. The ZnO sample obtained after the second thermal treatment, in white color (free of any organic material), was macerated towards a more homogeneous material.

### 2.2. Manufacture of gas sensors

rGO-ZnO dispersions were prepared by adding 1, 2, and 5 % per volume of ZnO dispersion (1 mg/mL) into the rGO dispersion (0.2 mg/mL) in distilled water. Both rGO and rGO-ZnO dispersions were sonicated for 30 min and deposited by drop-casting on the interdigitated electrodes, Fig. 1 (a). The sensors were named rGO, rGO-1%ZnO, rGO-2%ZnO, and rGO-5%ZnO, respectively. Cr/Au interdigitated electrodes fabricated by ultraviolet lithography and Cu/Au deposition by sputtering were deposited on 70 μm thick PET films to manufacture gas sensors on a PET substrate, Fig. 1 (b).

### 2.3. Gas detection measurements

The sensitivity of flexible sensors was evaluated to NO<sub>2</sub> gas at different concentrations at room temperature. Two gold-coated tungsten needles made contacts, and a Keithley electrometer measured electrical resistance. The baseline was obtained with synthetic air (20 % oxygen and 80 % nitrogen) at a 100 mL/min flow rate; NO<sub>2</sub> gas was generated in an Owlstone V-OVG permeation system that controls the gas concentration based on the permeation rate as a function of tube temperature.

Measurements at concentrations below 1 ppm, humidity, selectivity, and bending tests were conducted at Universitat Rovira i Virgili laboratories. The gas sensor was placed in an airtight testing chamber for the measurements. A pure dry air atmosphere (99.999 % Air Premier Purity) was used during the sensing tests and as a carrier gas for the target gases. The overall flow was adjusted at 100 mL/min low rate by a set of mass-flow controllers (Bronkhorst High-Tech B.V., The Netherlands) and electro-valves. The sensor resistances were monitored by a multimeter (HP 34972 A, Agilent, USA) that registered the resistance changes induced by different concentrations of gases. The sensors were exposed to given concentrations of target gases for 30 min and subsequently stabilized for 60 min under dry airflow at RT (27 °C). For a p-type semiconductor, the relative response was set as  $R = [(R_{\text{gas}} - R_{\text{air}})/R_{\text{air}}] \cdot 100$  for reducing gases and  $R = [(R_{\text{air}} - R_{\text{gas}})/R_{\text{air}}] \cdot 100$  for oxidizing gases, where  $R_{\text{gas}}$  is the resistance when the sensor was exposed to the target gas, and  $R_{\text{air}}$  is the resistance under synthetic air [28,29].

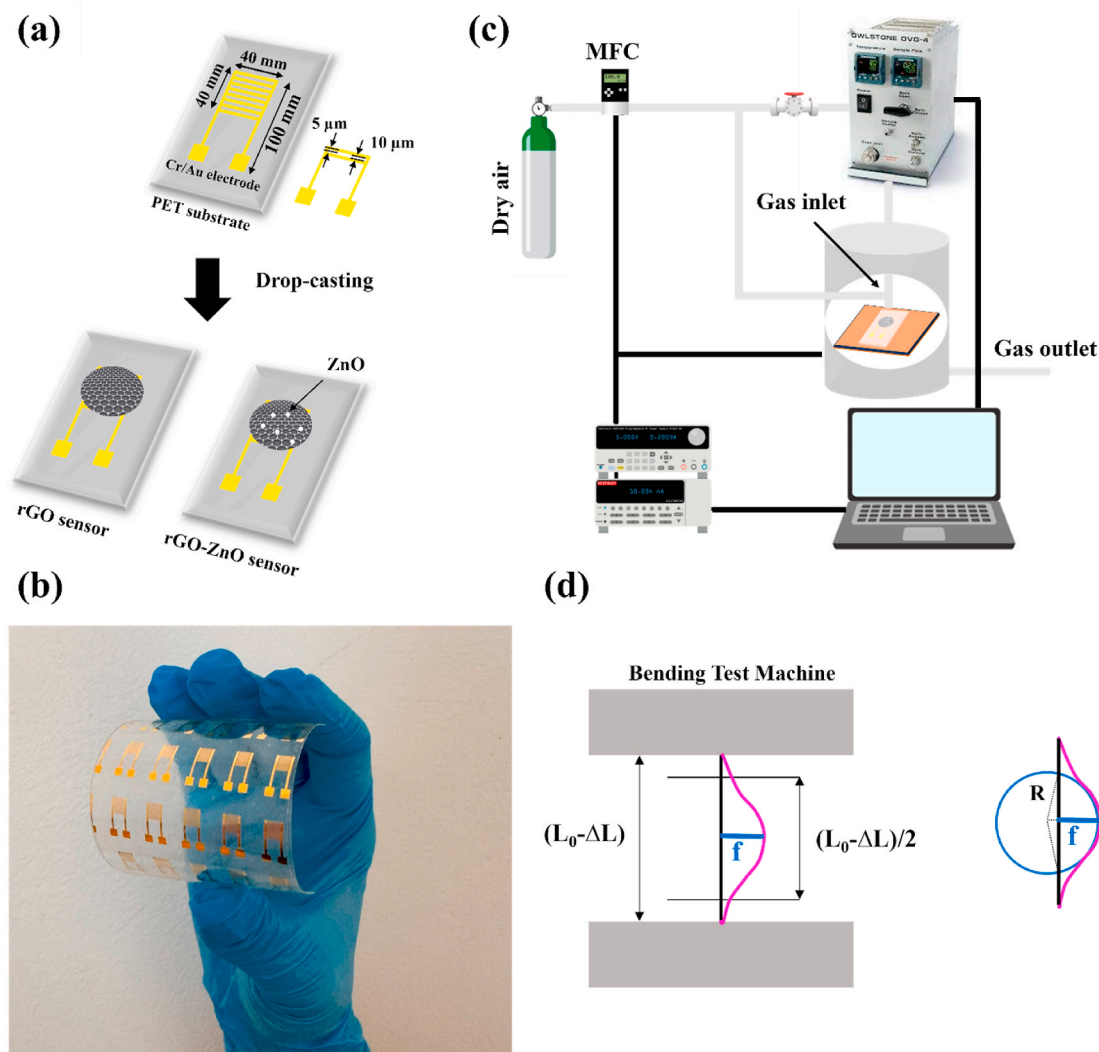


Fig. 1. (a) Fabrication methodology of flexible gas sensors made of rGO and rGO-ZnO, (b) Cu/Au interdigitated electrode on PET substrate, (c) schematic representation of the experimental apparatus used for NO<sub>2</sub> detection measurements and (d) schematic representation of the bending test under compression and the relationship between maximum deflection and radius of curvature of the sensor.

#### 2.4. Characterization

The structural characterization of ZnO was performed by X-ray diffraction technique (XRD) in a Rigaku Ultima IV diffractometer with CuK $\alpha$ 1 radiation ( $\lambda = 1.54056 \text{ \AA}$ ) and LiF monochromator (100) in the conventional  $\theta$ - $2\theta$  configuration. Raman spectroscopy characterized rGO under a Witec microscope with a highly linear stage and a Nikon objective lens (100xNA = 0.9). Raman spectra were obtained from the excitation of an Ar laser (488 nm; 10 mW) and Raman data were fitted by PeakFit software. The morphological characterization was performed by scanning electron microscopy (FEG-SEM). FEG-SEM images were obtained under a ZEISS model SIGMA scanning electron microscope with a field emission electron gun. The chemical characterization of rGO and rGO-ZnO sensors was conducted by X-ray photoelectron spectroscopy (XPS) in a Scienta Omicron ESCA + spectrometer, with Al K $\alpha$  monochromatic radiation (1486.7 eV), operated at incident power of 280 W beam and a charge neutralizer. The obtained data was adjusted using the CasaXPS software, calibrated by adventitious carbon binding energy (284.8 eV).

### 3. Results and discussion

#### 3.1. Structural characterization

Fig. 2 (a) shows the X-ray diffraction pattern of ZnO. All peaks are indexed to card JCPDS:36-1451, confirming the wurtzite phase of ZnO [10]. No other diffraction peaks corresponding to another crystalline phase or impurities were observed within the detection limit of the technique. XRD patterns of the rGO-ZnO heterostructures were performed; however, due to the low concentration of ZnO (1, 2 and 5 % volume), none of the ZnO peaks were identified, and the diffractograms will not be presented.

The Raman spectra of rGO and rGO-ZnO films were obtained within a 200–3500  $\text{cm}^{-1}$  range; the results are shown in Fig. 2 (b). The prominent bands of rGO are D, G, and 2D. G band ( $\sim 1580 \text{ cm}^{-1}$ ) is a stretching mode of  $\text{sp}^2$  carbon and exists for all C-C  $\text{sp}^2$  systems [30]. 2D band ( $\sim 2700 \text{ cm}^{-1}$ ), also known as G', is a second-order band related to the breathing mode in the plane of carbon rings [30,31]. 2D is linked to the electronic band structure of graphene materials and changes as the band structure of the material changes. Therefore, G and 2D are active and satisfy the Raman selection rules [32].

D ( $\sim 1350 \text{ cm}^{-1}$ ) occurs when the electron is inelastically scattered by an iTO phonon to the K' point and then elastically backscattered to

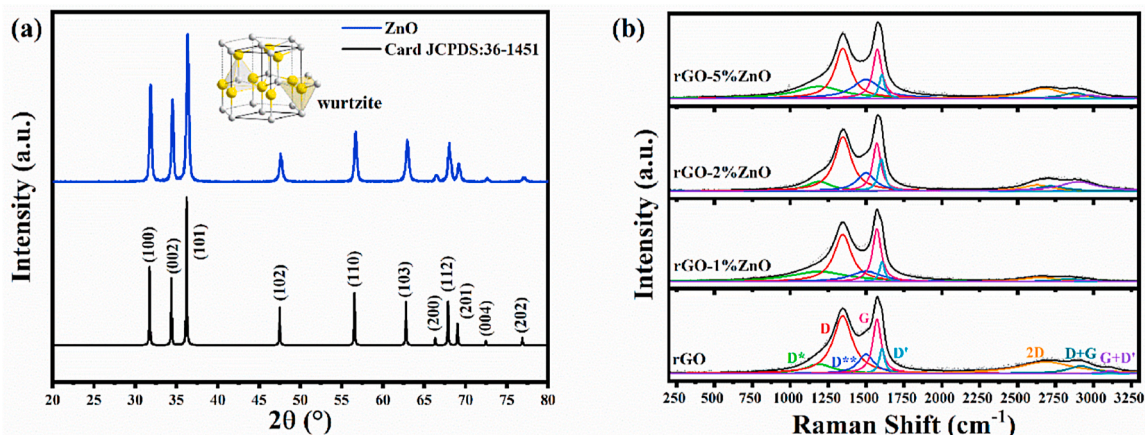


Fig. 2. (a) X-ray diffraction pattern of ZnO and (b) Raman spectrum of rGO and rGO-ZnO films.

the K point by a defect. Since only one phonon is involved, D has half the frequency of 2D [30,33] and, since D is associated with defects in the material structure, the  $I_D/I_G$  ratio has been extensively studied for the characterization of disordered carbon content, defects, and  $sp^3/sp^2$

fraction in carbon-based materials [34]. Therefore,  $I_D/I_G$  ratio is a good estimate of the density of defects in the material [35] – it is 1.05 for rGO in Fig. 2 (b), in agreement with the literature [36]. The  $I_D/I_G$  values for rGO-ZnO heterostructures with 1, 2, and 5 % ZnO are 0.89, 1.13, and

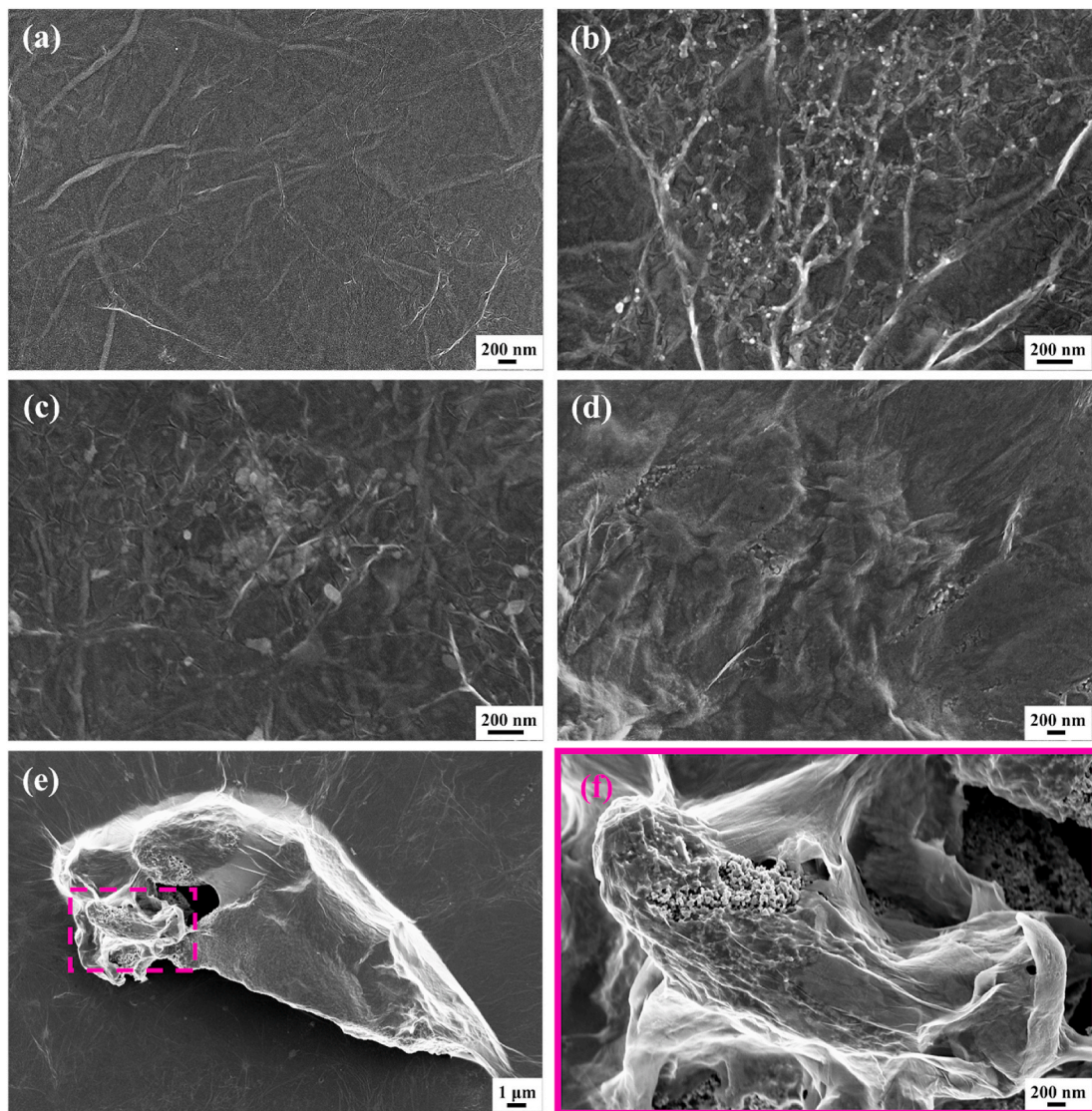


Fig. 3. SEM images of flexible gas sensors of (a) rGO, (b) rGO-1%ZnO, (c) rGO-2%ZnO and (d)–(f) rGO5%ZnO.

1.01, respectively.  $I_{2D}/I_G$  is another significant ratio in the Raman characterization of carbon materials and reflects the density of the “graphenization” extension, i.e., a structure like pristine graphene [33, 37]. It can also predict the charge carrier mobility [38]. It is 0.21 for the studied rGO, and the values for rGO-ZnO heterostructures with 1, 2, and 5 % ZnO are 0.08, 0.12, and 0.20, respectively, suggesting the initial addition of ZnO nanoparticles reduced the mobility of charge carriers and the material’s electronic properties; however, with the increase in % v/v of ZnO, the  $I_{2D}/I_G$  ratio also increased.

In the Raman spectrum, peaks associated with ZnO are observed between 100 and 1000  $\text{cm}^{-1}$ , with prominent ones centered at 99  $\text{cm}^{-1}$  and 437  $\text{cm}^{-1}$  [39]. However, they were not detected in the Raman spectrum of the heterostructures due to the low concentration of ZnO used to form them. It is known that MOS-based sensors typically operate at high temperatures; therefore, heterostructures with low concentrations of ZnO were explored in this work.

### 3.2. Morphological characterization

Fig. 3 (a) shows the rGO sensor with a relatively smooth surface with some folds due to the stacking of rGO sheets. Fig. 3 (b) depicts a micrograph of rGO-1%ZnO sensor, with rGO sheets completely covering the PET substrate and ZnO nanoparticles (light spots) decorating rGO sheets in the region of the folds of those sheets. Fig. 3 (c) shows the micrograph of rGO-2%ZnO sensor, where a morphology like that of the sensor with 1 % ZnO can be observed. However, in addition to being anchored on the surface of rGO sheets, ZnO nanoparticles are surrounded by them. Fig. 3(d)–(f) displays the micrographs of rGO-5%ZnO sensor at different magnifications. Fig. 3 (d) shows ZnO nanoparticles anchored on the surface of rGO sheets and enveloped by them. The sensor containing 5 % ZnO also formed clusters of ZnO nanoparticles

surrounded by rGO sheets, Fig. 3 (e). Fig. 3 (f) displays the magnification of a cluster region identified in Fig. 3 (e).

### 3.3. XPS analysis

Fig. 4a depicts the survey spectra of rGO and rGO-ZnO sensors on PET substrate. The rGO spectrum displays peaks associated with S 2p (166.5 eV), C 1s (283.5 eV), O 1s (530.5 eV), and Na 1s (1070.5 eV). Na and S are impurities incorporated into the material during the GO chemical reduction process. A peak related to Zn 2p (1020.5 eV) was also identified in the spectra of rGO-ZnO heterostructures. Table A.1 in the supplementary data shows the atomic % concentration of all elements in each sample. The concentration of Zn increases as the percentage of ZnO increases in the sensor, being 0.3, 0.46, and 1.57 % at% for the rGO-1%ZnO, rGO-2%ZnO and rGO-5%ZnO sensors, respectively.

The C 1s spectrum of rGO sensor, Fig. 4 (b), was deconvoluted into five bands related to the bonds of C  $\text{sp}^2$  (284.69 eV), C  $\text{sp}^3$  (285.45 eV), C-O (286.50 eV), C=O (287.88 eV), and COOH (289.67 eV) [40]. Among the five bands in the spectrum, the one associated with C  $\text{sp}^2$  has the highest concentration (70.58 wt%), due to the restoration of  $\text{sp}^2$  carbon domains after the chemical reduction of GO. However, there is still a tiny amount of residual oxygenated functional groups in GO characterized by the presence of other bands in the spectrum. The O 1s spectrum of rGO sensor, Fig. 5 (c), was deconvoluted into three components attributed to C=O (530.25 eV) of PET [41], C=O (531.3 eV) of rGO and C-O of rGO (532.3 eV), in agreement with the literature [42].

Fig. 5(a)–(c) displays the high-resolution C 1s spectra of rGO-ZnO sensors on PET substrate. Like what was observed on the rGO sensor, the C 1s spectra were deconvoluted into five components attributed to C  $\text{sp}^2$  (284.7 eV), C  $\text{sp}^3$  (285.4 eV), C-O (286.4 eV), C=O (287.4 eV), and COOH (289.4 eV) bonds. Fig. 5(d)–(f) shows the high-resolution O 1s

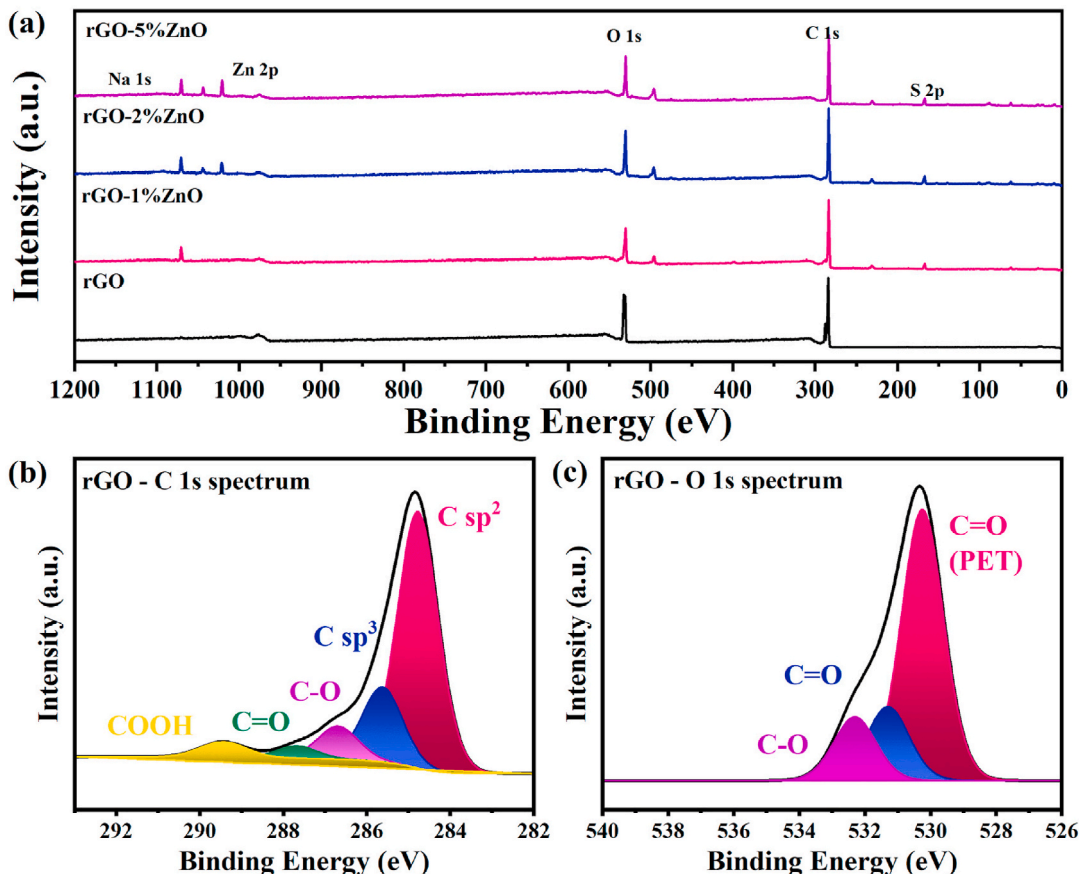


Fig. 4. – (a) Survey XPS spectra of rGO and rGO-ZnO heterostructure samples, (b) high-resolution C 1s spectrum of rGO and (c) high-resolution O 1s spectrum of rGO.

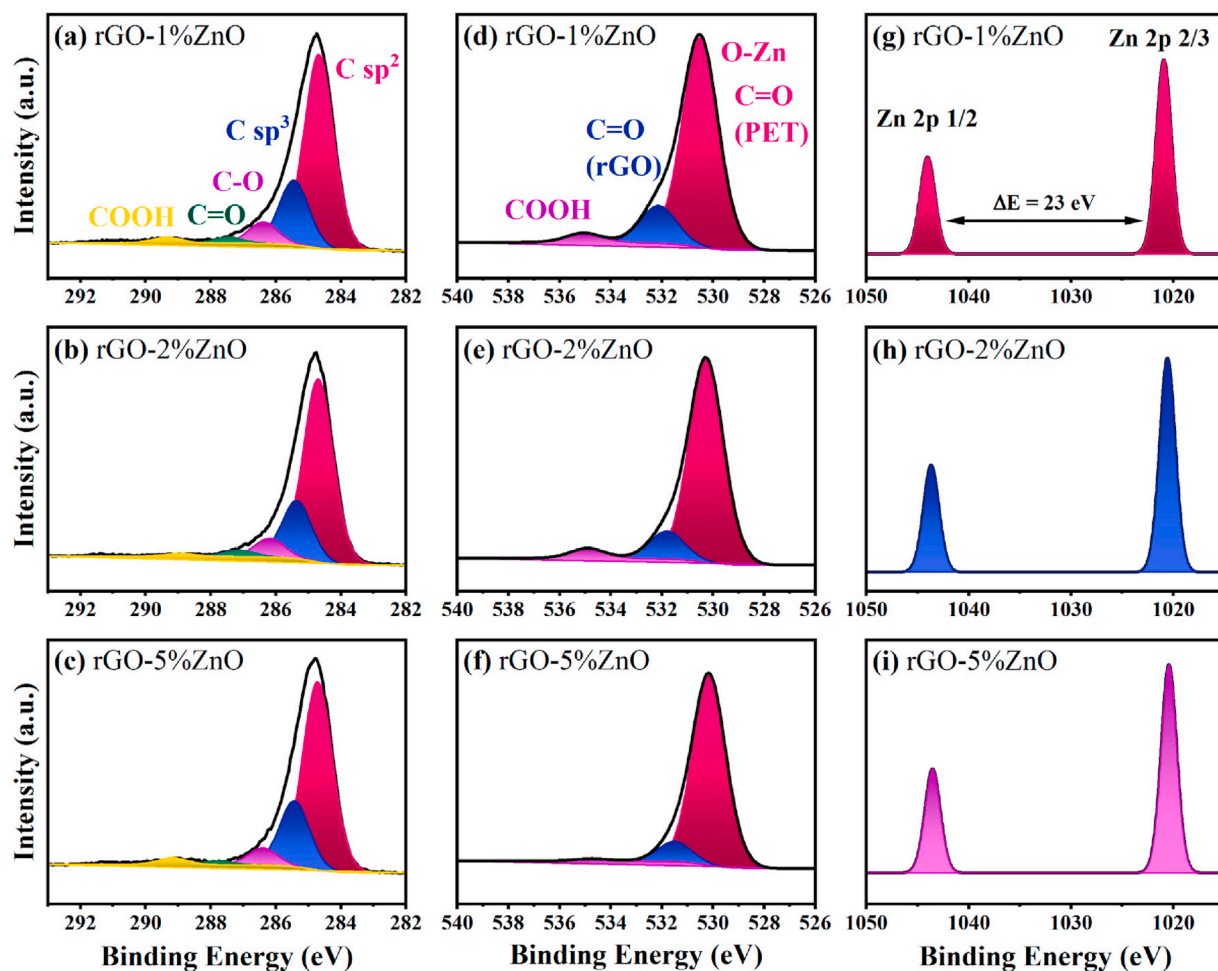


Fig. 5. – High-resolution C 1s spectra of (a) rGO-1%ZnO, (b) rGO-2%ZnO, and (c) rGO-5%ZnO samples, high-resolution O 1s spectra of (d) rGO-1%ZnO, (e) rGO-2% ZnO, and (f) rGO-5%ZnO samples, and high-resolution Zn 2p spectra of (g) rGO-1%ZnO, (h) rGO-2%ZnO, and (i) rGO-5%ZnO samples.

spectra of rGO-ZnO sensors. The O 1s spectra were deconvoluted into three components, at 530.5 eV attributed to O-Zn bonds [43] and C=O of PET substrate, a second component around 531.5 eV, refers to C=O bond of rGO, and the third component, around 535 eV, is attributed to COOH bond of rGO [42]. The high-resolution spectra of Zn 2p for rGO-ZnO sensors presented in Fig. 5(g)–(i) show peaks around 1021 and 1044 eV, corresponding to Zn 2  $p_{3/2}$  and Zn 2  $p_{1/2}$  levels, respectively [44]. The energy variation ( $\Delta E$ ) between these peaks was 23 eV, indicating the presence of  $Zn^{2+}$  in all samples [45]. ZnO is known to present high chemical, thermal and structural stability [12], therefore, there was no modification in the signal of the high-resolution spectrum of Zn with the formation of the rGO-ZnO heterostructure.

### 3.4. Gas detection

The rGO and rGO-ZnO sensors were exposed to different concentrations of  $NO_2$  (1.5, 2.0 and 2.5 ppm) at room temperature, Fig. 6. The exposure time to the gas was 30 min, and the recovery time was 60 min. When exposed to  $NO_2$ , the electrical resistance of the sensors is reduced, demonstrating a typical behavior of p-type semiconductors in an oxidizing gas due to the high concentration of rGO in the heterostructure.

For comparison purposes, the dynamic response-recovery curves were normalized and plotted on the same graph, Fig. 7 (a), and the sensor responses were plotted as a function of  $NO_2$  concentration, Fig. 7 (b). When exposed to 1.5 ppm of  $NO_2$ , rGO, rGO-1%ZnO, rGO-2%ZnO, and rGO-5%ZnO sensors display responses of 5.6 %, 16.7 %, 16.9 %, and

18.5 %, respectively, showing the effect of ZnO addition on the sensor response, when compared to rGO sensor. The response time is defined as the time a sensor spends to reach 90 % of maximum resistance when exposed to a target gas [28]. Fig. 7 (c) depicts the response time of rGO and rGO-ZnO sensors as a function of  $NO_2$  concentration. The response times of rGO, rGO-1%ZnO, rGO-2%ZnO, and rGO-5%ZnO sensors are 20.9, 17.01, 16.3, and 14.2 min, respectively, to 1.5 ppm of  $NO_2$ , exhibiting a significant reduction when compared to the rGO sensor. However, the recovery time of rGO-ZnO increases since MOS, such as ZnO, typically operates at high temperatures ( $>200$  °C) due to the thermal energy required to initiate redox reactions at the sensing surface [10]. The next gas sensor characterizations were only performed on the rGO-5%ZnO sensor since it presented the highest response and the lowest response time.

The sensitivity of a sensor is defined as the angular coefficient of the straight line obtained by the linear fit of the response results by the concentration of the target gas [28]. As can be seen in Fig. 7 (d), the rGO-5%ZnO sensitivity was 3.9 %/ppm, while that of rGO was 1.7 %/ppm.

The limit of detection (LOD) is defined as the minimum concentration of gas that a sensor can detect. The LOD can be calculated by  $LOD = 3S/N$ , where S is the standard deviation of the sensor baseline and N is the slope of the fitting of the graph of response versus gas concentration, also called sensor sensitivity [28]. Being  $S = 0.003$  and  $N = 3.9$ , we have that the LOD of the rGO-5%ZnO sensor is 0.002 ppm or 2 ppb.

In addition to response and recovery times, stability, selectivity, and influence of humidity are also fundamental parameters for a gas sensor.

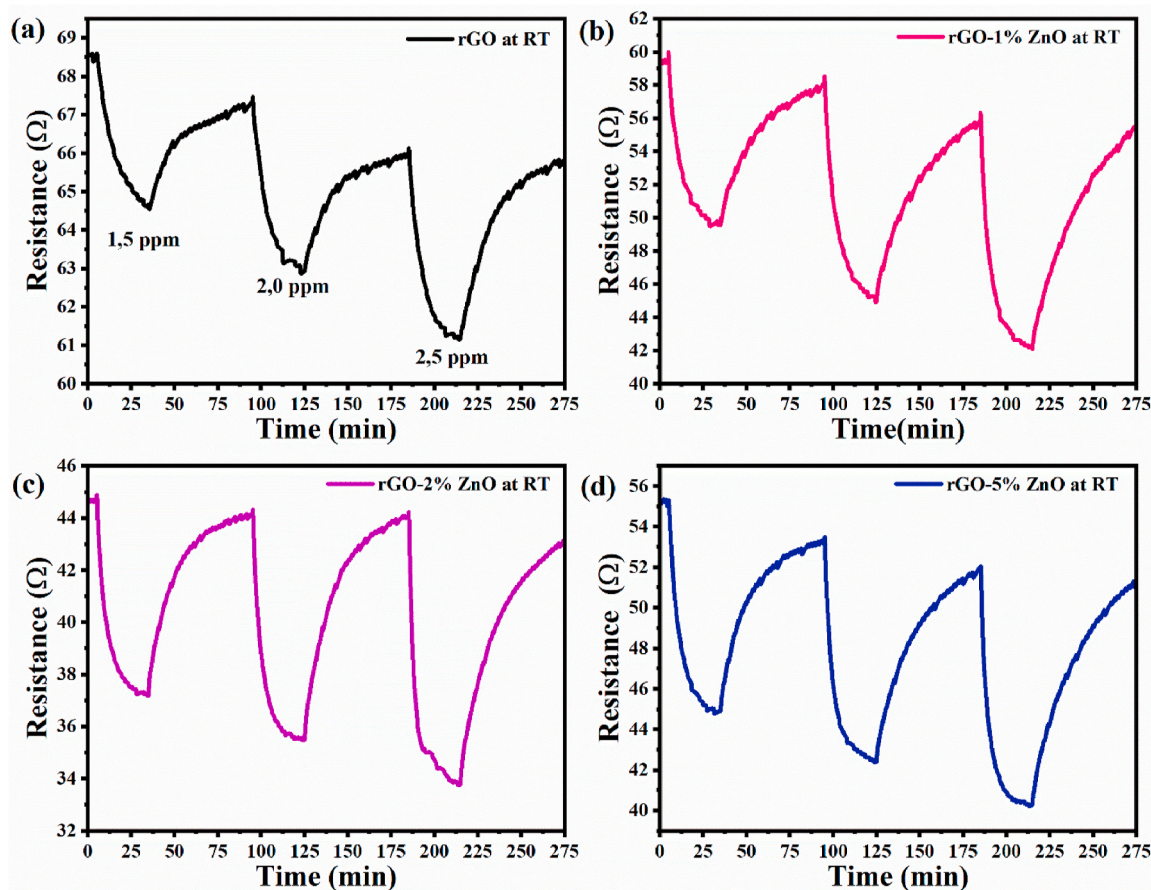


Fig. 6. – Dynamic response-recovery curves for NO<sub>2</sub> detection at room temperature for (a) rGO, (b) rGO-1%ZnO, (c) rGO-2%ZnO, and (d) rGO-5% ZnO sensors.

Humidity, selectivity, stability and flexural test measurements were carried out in the Universitat Rovira I Virgili (URV) laboratories in Spain. As a result, gas chamber size, type of electrical contact, and direction of gas flow changed. Such factors influence the response of the gas sensors, causing changes in their responses. Since the results will not be compared with previous measurements, the discussions held in this study will not be affected.

Humidity is a critical parameter for gas sensors operating at room temperature. NO<sub>2</sub> detection measurements with 10 %, 30 %, 50 %, and 70 % humidity were conducted to evaluate the effect of humidity on the rGO-5%ZnO sensor. Fig. 8 (a) displays the dynamic response-recovery curves in dry and humid air, and as can be observed, the dry air curve does not show a complete recovery; however, when exposed to humidity, it shows a full recovery for all evaluated humidity levels. Fig. 8 (b) depicts the response (%) of the rGO-5%ZnO sensor in dry and humid air, showing an increase when the sensor is exposed to 10–50 % humidity and no significant change above 50 %. Such an increase in the response of rGO-ZnO sensors exposed to NO<sub>2</sub> with humidity was also reported in the literature [12,46]. Fig. 8 (c) displays the response times of the sensors in dry and humid air. When exposed to 10 % humidity, the sensors show an excellent reduction in response time, and when humidity increases to 30 and 50 %, the response times increase but remain lower compared to dry air sensors. When humidity rises to 70 %, the sensors' response is lower than at 30 and 50 %. Such a reduction in sensor response in a highly humid environment results from ionic electrical signal conduction through water molecules adsorbed on the sensor surface [8]. Fig. 8 (d) shows the sensor recovery times in dry and humid air. As discussed elsewhere, rGO-5%ZnO does not entirely recover when exposed to NO<sub>2</sub> in dry air; however, when exposed to NO<sub>2</sub> with 10 % humidity, it shows a rapid recovery (~10 min). Similar results

were reported by Kang et al. (2021) in which the response of a Pt/ZnO/PRGO sensor to 5 ppm NO<sub>2</sub> under conditions of 1.5 %–90 % humidity was evaluated [8].

To evaluate the selectivity of the rGO-5%ZnO sensor relative to other gases, the sensor was exposed to different gases at RT, and the responses are presented in Fig. 9 (a). When comparing the sensor response to other gases, this sensor presents high selectivity to NO<sub>2</sub>, which can be attributed to the high absorption energy of NO<sub>2</sub> with rGO-ZnO [10]. Due to the lower binding energy, high adsorption capacity, and high surface reactivity, rGO-5%ZnO shows high sensitivity to NO<sub>2</sub> gas compared to the other gases explored. The relative response of the sensor was normalized by comparing NO<sub>2</sub> with the different gases. The normalized response is given by the equation  $R_{nor} = R_{gas}/R_{NO_2}$ , where  $R_{gas}$  is the relative response of the sensor to an analyte and  $R_{NO_2}$  is the relative response of the sensor to NO<sub>2</sub> [47]. The  $R_{nor}$  was 0.018 (CO), 0.011 (H<sub>2</sub>), 0.003 (NH<sub>3</sub>), 0.042 (toluene), 0.031 (benzene), and 0.007 (ethanol). These results demonstrate the strong selectivity of the rGO-5%ZnO sensor to NO<sub>2</sub>, while it exhibited negligible response to the other gases. The stability over time of the rGO-5%ZnO sensor was evaluated by periodic measurements of 1 ppm NO<sub>2</sub> over 7 days, Fig. 9 (b). The sensor performs well over the observed period, in good agreement with the literature [10,48].

Bending tests assessed the rGO-5%ZnO sensor's applicability as a flexible gas sensor to determine the electrical resistance behavior during the tests and the sensing properties before and after bending. Fig. 10(a) and (b) and Fig. 10(d) and (e) show the electrical behavior of the rGO-5%ZnO sensor over several bending cycles in compressive strain with strokes of 0.2 and 0.4 mm. When the sensor is bending in a compressive strain, the electrical resistance increases and returns to near baseline when the compressive strain is removed. After 100 bending cycles in a

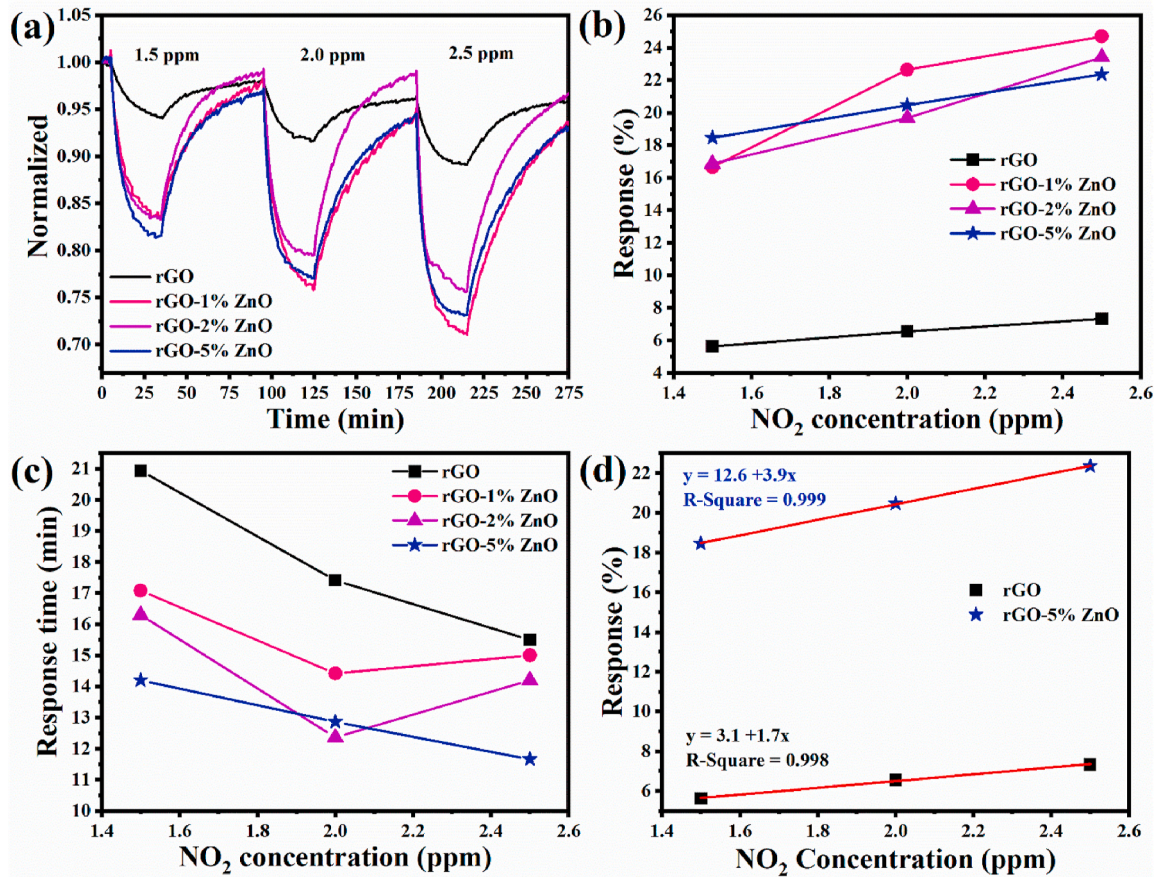


Fig. 7. – (a) Normalized dynamic response-recovery curves of rGO and rGO-ZnO sensors, (b) response (%) as a function of NO<sub>2</sub> concentration, (c) response time as a function of NO<sub>2</sub> concentration, and (d) Linear fit of response line (%) versus NO<sub>2</sub> concentration.

compressive strain, the sensor's electrical resistance showed no significant variation, indicating that the sensor was not damaged during bending cycles.

To evaluate whether the bending cycles applied to the sensor affected its sensing properties, NO<sub>2</sub> detection measurements were performed before and after the bending test. Fig. 10 (g) shows the equipment used for the bending test and the sensor before (linear) and during compressive strain. S1 sensor was submitted to 100 bending cycles with a stroke of 0.2 mm, and the S2 sensor was submitted to 100 bending cycles with a stroke of 0.2 mm and 0.4 mm. The response of sensors S1 and S2 before and after the bending test are shown in Fig. 10 (c) and (f). No significant variation in the sensor response was detected after the bending cycles, demonstrating that the compressive strain did not affect the sensing properties of the gas sensors and that the rGO-5%ZnO sensor on PET substrate exhibits high flexibility. The curvature angle and maximum deflection of the sensor were calculated and are presented in topic B.2 of the supplementary data.

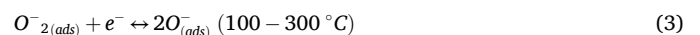
Table 1 summarizes the sensing properties of flexible NO<sub>2</sub> sensors using a PET substrate developed during this study, compared to findings from existing literature. Compared to the literature, our results demonstrate that the rGO-5%ZnO sensor presents a high response (22.4 %), high stability, and good selectivity to NO<sub>2</sub> and allows the detection of low concentrations of NO<sub>2</sub>. In addition, our sensor presents high flexibility, indicating that it can be incorporated into clothing and accessories for real-time monitoring of air conditions.

### 3.5. Sensing mechanism

The band structure of the pure materials and rGO-5%ZnO heterostructure can be built with the materials' work function (WF) and

bandgap values. Figure A (supplementary data) presents the UPS spectra of the rGO, ZnO and rGO-5%ZnO films and UV-Vis for the rGO and ZnO films. Through these results, the WF and bandgap values can be obtained. Fig. 11 (a) illustrates the band structure of rGO and ZnO before forming the heterostructures, and Fig. 11 (b) shows the band structure of rGO-5%ZnO heterostructure.

The most conventional gas detection mechanism for MOS is based on the oxygen adsorption model [51], which is based on the variation in electrical resistance after exposure to the target gas due to chemical interactions between the target gas and oxygen ions adsorbed on the material's surface. The operating temperature of the sensor determines the type of oxygen ions chemisorbed. Equations (1)–(4) show the formation process of chemisorbed oxygen ions in each temperature range [52].



The type of semiconductor, p or n, defines the sensors' detection mechanism. For an n-type, the mechanism depends on most carrier electrons, whereas in the p-type, it depends on the hole carrier density [18]. In this study, rGO-ZnO sensors display a p-type behavior similar to rGO. rGO has excellent electrical conductivity, showing a conductive path for an efficient transport of charge carriers. ZnO, an n-type material, is non-negligible in achieving high sensor responses [9]. Therefore, forming a p-n heterojunction significantly affects the performance of



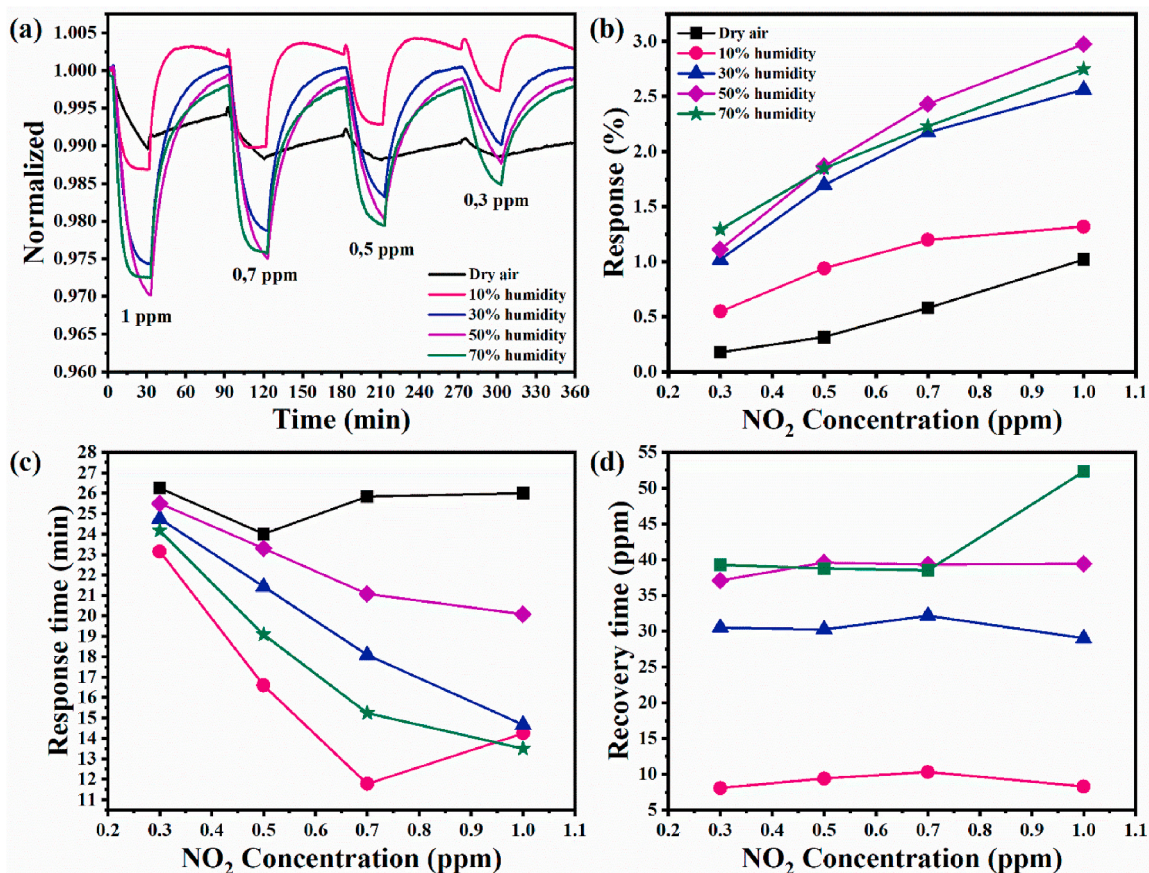


Fig. 8. – (a) Dynamic response-recovery curves for NO<sub>2</sub> under dry air conditions and different humidity levels of rGO-5%ZnO sensor, (b) response (%) as a function of NO<sub>2</sub> concentration under dry air conditions and different humidity levels, and (c) response time and (d) recovery time under dry air conditions and different humidity levels.

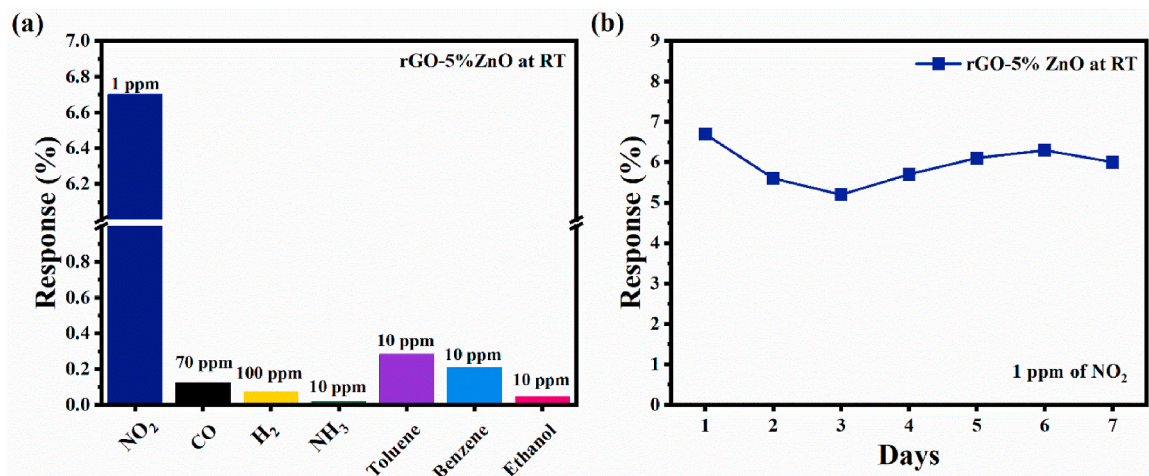
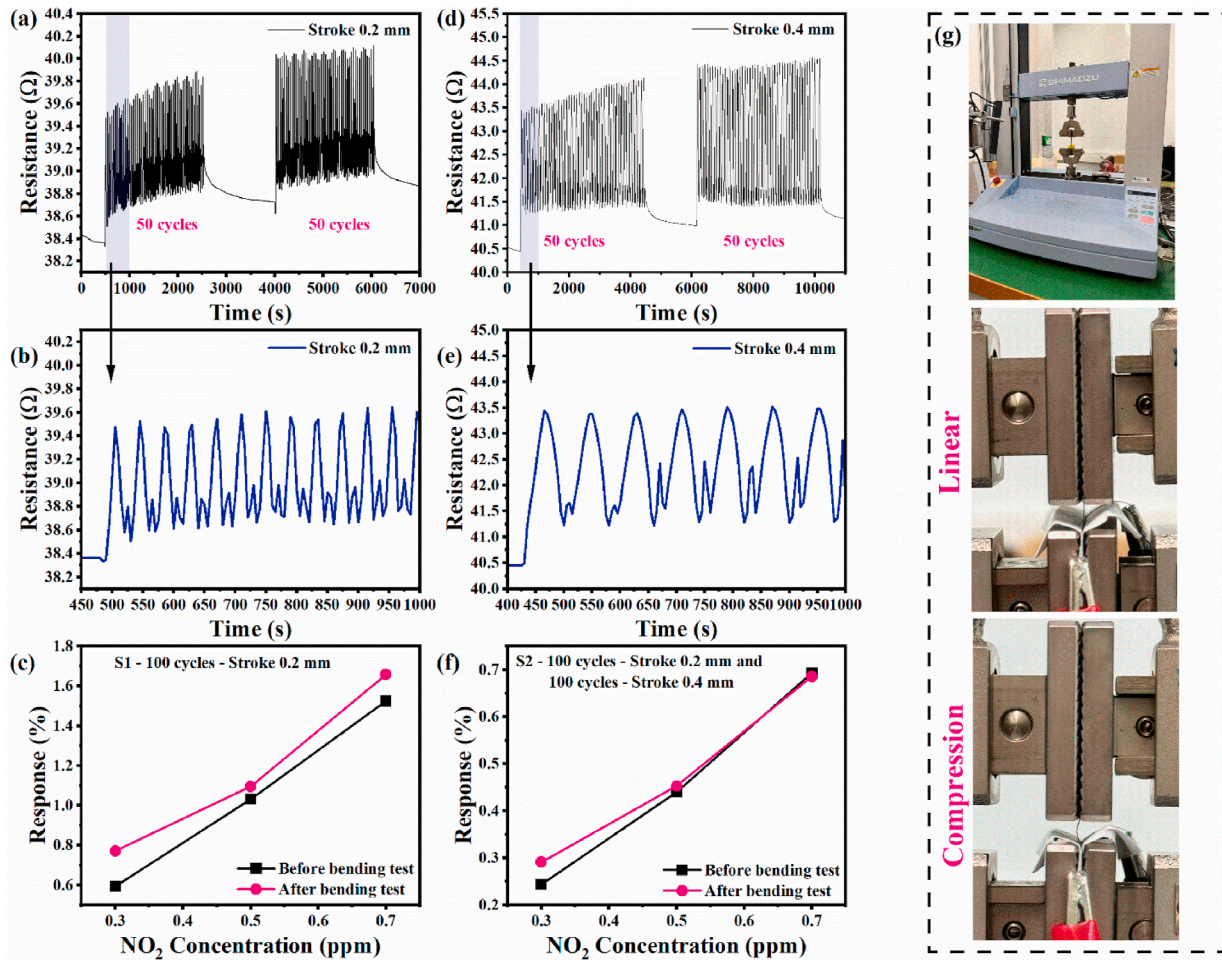


Fig. 9. – (a) selectivity of rGO-5%ZnO sensor at RT and (b) stability over time at RT.

rGO-ZnO sensors [12]. Since the Fermi levels of ZnO are different, rGO acts as an electron acceptor for extracting electrons from the ZnO surface and equalizing the Fermi level, resulting in a smaller number of electrons at the surface and interface of ZnO, hence, a higher potential barrier and a more significant depletion layer [53].

When the sensor is exposed to air at room temperature, oxygen molecules are adsorbed on the surface of rGO-ZnO, Eqs (1) and (2), capturing electrons from the conduction band of ZnO, which leads to an increase in the electron depletion layer and a curvature in the band [9].

When the sensor is exposed to NO<sub>2</sub>, electrons are transferred from rGO-ZnO to the adsorbed NO<sub>2</sub> molecules Eq (5), and, since the electronegativity of NO<sub>2</sub><sup>-</sup> is greater than that of O<sub>2</sub><sup>-</sup>, they react to forming NO<sub>3</sub><sup>-</sup>, Eq (6) [54]. The reduction of electrons in ZnO after NO<sub>2</sub> adsorption decreases the Fermi level, leading to a charge transfer between ZnO and rGO. As a result, rGO transfers electrons to ZnO, thus increasing the concentration of holes in rGO, which reduces the electrical resistance of rGO-ZnO when exposed to NO<sub>2</sub>. Electrons from rGO are also transferred to NO<sub>2</sub>, Eq (7), which further reduces the sensor's electrical resistance,



**Fig. 10.** – (a)–(b) Variation of the electrical resistance of the rGO-5%ZnO sensor during 100 bending cycles with 0.2 mm stroke, (c) response (%) as a function of the NO<sub>2</sub> concentration before and after 100 bending cycles with 0.2 mm stroke, (d)–(e) variation of the electrical resistance of the rGO-5%ZnO sensor during 100 bending cycles with 0.4 mm stroke, (f) response (%) as a function of the NO<sub>2</sub> concentration before and after 100 bending cycles with 0.2 mm stroke and 100 cycles with 0.4 mm stroke and (g) equipment used in the bending test.

**Table 1**

Comparison of the sensor properties of flexible NO<sub>2</sub> sensor using PET substrate from this study with the literature results.

Sensor	NO <sub>2</sub> (ppm)	Response (%)	T <sub>res</sub> / T <sub>rec</sub>	Flexibility <sup>a</sup>	Stability	Ref
rGO-5%ZnO	2.5	22.4	12 min/-	Yes	7 days	This work
WO <sub>3</sub> / MWCNTs	5.0	14	10 min/ 27 min	Yes	–	[2]
rGO	5.0	11.5	7 min/ 28 min	Yes	43 days	[15]
WO <sub>3</sub> / MWCNT- rGO	5.0	17	7 min/ 15 min	Yes	–	[16]
MoS <sub>2</sub> /CNT	40	54	–	Yes	–	[17]
Polypyrrole/ SnO <sub>2</sub>	5.0	8.2	–	–	–	[49]
NbSe <sub>2</sub> /WSe <sub>2</sub>	5	30	–	Yes	–	[50]

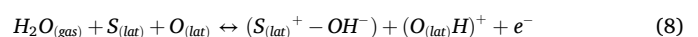
<sup>a</sup> The sensors have undergone some bending testing.

improving response, as can be seen in Fig. 6 (a) [8,10].



The formation of a p-n heterojunction provides more adsorbed oxygens on the sensor surface, acting as active sites to interact with NO<sub>2</sub> and increasing the sensor response. In addition, it is known that rGO sheets have a high surface area, causing ZnO NPs to quickly stabilize, forming a good contact between ZnO and rGO [10]. Because ZnO has a lower work function, Fig. 11 (a), rapid charge transfer occurs between ZnO and rGO, which improves the sensor response and decreases the response time. rGO also presents several defects, such as oxygen vacancies and oxygenated functional groups that provide more active sites and enable the sensor to operate at room temperature.

When rGO-ZnO is exposed to NO<sub>2</sub> under humid conditions, the interaction of water vapor with the material's surface generates an increase in bridging hydroxyl groups and the formation of terminal OH groups. To achieve this, dissociative water adsorption occurs on the material's metal atoms (Zn), giving rise to terminal OH groups and hydrogen atoms that bind to the family of bridged hydroxyls. Such a formation of hydroxyls is described by Eq (8) [55,56].



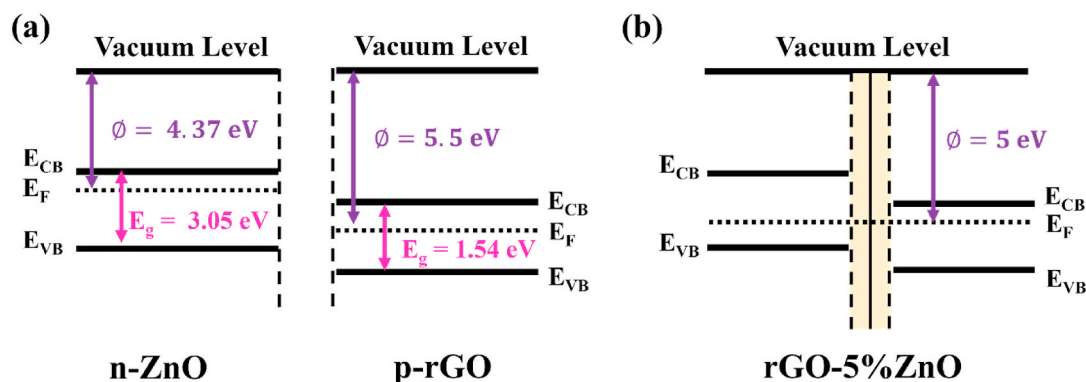
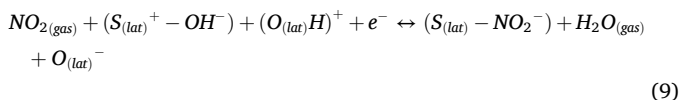


Fig. 11. – Band structure of samples of (a) pure ZnO and rGO and (b) rGO-5%ZnO heterostructure.

At low temperatures (<150 °C), NO<sub>2</sub> is adsorbed on the surface of the material in hydroxyls, and nitrites are formed [57]. The NO<sub>2</sub> absorption on the surface of a metal oxide semiconductor, ZnO, in a humid environment can be described by Eq (9) [55].



As discussed above, in dry air conditions, NO<sub>2</sub> is adsorbed on the material's surface by interaction with the oxygen ions present. Now in a humid environment, in addition to the adsorbed oxygen ions, hydroxyls are generated by the presence of water vapor [57]. This causes more electrons to be extracted from the conduction band of ZnO, further reducing its Fermi level. More electrons from rGO are transferred to ZnO to balance Fermi levels, thus increasing the number of vacancies on the rGO surface and further reducing sensor resistance. As a result, the response of rGO-ZnO sensor is increased. Therefore, the “wet” surface is beneficial for adsorbing a greater quantity of NO<sub>2</sub> and is consequently responsible for greater sensitivity in detecting NO<sub>2</sub> at room temperature. The water-mediated enhanced adsorption of NO<sub>2</sub> on ZnO [46] and In<sub>2</sub>O<sub>3</sub> [57] surfaces has been reported previously.

#### 4. Conclusions

XPS analysis of the rGO-ZnO heterostructure reveals an increased concentration of Zn in the ZnO. At the same time, FEG-SEM imaging shows that ZnO nanoparticles are anchored on the rGO surface and surrounded by rGO sheets. Gas detection measurements indicate that both rGO and rGO-ZnO sensors are sensitive to NO<sub>2</sub> at room temperature, with the rGO-5% ZnO sensor exhibiting the best sensing performance, achieving a response of 18.5 % at 1.5 ppm NO<sub>2</sub> and demonstrating high selectivity for NO<sub>2</sub>. Interestingly, exposure to humidity enhances both the response and recovery times, suggesting its suitability for real-world environmental conditions. Additionally, the sensor displayed strong stability during bending tests involving multiple compression cycles. These findings highlight the potential of this flexible gas sensor for NO<sub>2</sub> detection at room temperature.

#### CRedit authorship contribution statement

**Amanda Akemy Komorizono:** Writing – original draft, Visualization, Methodology, Investigation, Conceptualization. **Ramon Resende Leite:** Writing – review & editing, Validation, Investigation. **Silvia De la Flor:** Writing – review & editing, Methodology. **Eduard Llobet:** Writing – review & editing, Supervision, Resources. **Valmor Roberto Mastelaro:** Writing – review & editing, Supervision, Resources, Project administration, Funding acquisition.

#### Declaration of competing interest

The authors declare that they have no known competing financial interests or personal relationships that could have appeared to influence the work reported in this paper.

#### Acknowledgments

This research was supported by the Sao Paulo Research Foundation's financial support – FAPESP (grants number 2013/07296–2, 2019/22076–5, 2022/03325–7 and 2023/00913–8), the Brazilian National Science Financial Agencies CNPq (grants number 307231/2021–6), and Capes. The authors acknowledge the Microfabrication Laboratory at the Brazilian Nanotechnology National Laboratory (LNNano-CNPq), Campinas, SP, Brazil (Project LMF-20232214 and LMF-20240100). E.L. was supported by the Catalan Institution for Research and Advanced Studies via the 2023 Edition of the ICREA Academia Award.

#### Appendix A. Supplementary data

Supplementary data to this article can be found online at <https://doi.org/10.1016/j.mssp.2024.109229>.

#### Data availability

No data was used for the research described in the article.

#### References

- [1] S. Drewniak, E. Drewniak, T. Pustelny, Mechanisms of NO<sub>2</sub> detection in hybrid structures containing reduced graphene oxide: a review, *Sensors* 22 (2022), <https://doi.org/10.3390/s22145316>.
- [2] U. Yaqoob, D. Phan, A.S.M.I. Uddin, G. Chung, Highly flexible room temperature NO<sub>2</sub> sensor based on MWCNTs-WO<sub>3</sub> nanoparticles hybrid on a PET substrate, *Sensor. Actuator. B Chem.* 221 (2015) 760–768, <https://doi.org/10.1016/j.snb.2015.06.137>.
- [3] J. Liu, S. Li, B. Zhang, Y. Xiao, Y. Gao, Q. Yang, Y. Wang, G. Lu, Ultrasensitive and low detection limit of nitrogen dioxide gas sensor based on flower-like ZnO hierarchical nanostructure modified by reduced graphene oxide, *Sensor. Actuator. B Chem.* 249 (2017) 715–724, <https://doi.org/10.1016/j.snb.2017.04.190>.
- [4] N. Wang, W. Tao, X. Gong, L. Zhao, T. Wang, L. Zhao, F. Liu, X. Liu, P. Sun, G. Lu, Highly sensitive and selective NO<sub>2</sub> gas sensor fabricated from Cu<sub>2</sub>O-CuO microflowers, *Sensor. Actuator. B Chem.* 362 (2022) 131803, <https://doi.org/10.1016/j.snb.2022.131803>.
- [5] R. You, D.D. Han, F. Liu, Y.L. Zhang, G. Lu, Fabrication of flexible room-temperature NO<sub>2</sub> sensors by direct laser writing of In<sub>2</sub>O<sub>3</sub> and graphene oxide composites, *Sensor. Actuator. B Chem.* 277 (2018) 114–120, <https://doi.org/10.1016/j.snb.2018.07.179>.
- [6] Y. Yang, Z.D. Deng, Stretchable sensors for environmental monitoring, *Appl. Phys. Rev.* 6 (2019), <https://doi.org/10.1063/1.5085013>.
- [7] S. Dutta, S. Kumar, Y. Yu, H. Rubahn, Y. Kumar, K. Awasthi, Functional nanomaterials in flexible gas sensors: recent progress and future prospects, *Mater. Today Chem.* 29 (2023) 101428, <https://doi.org/10.1016/j.mtchem.2023.101428>.
- [8] J. Kang, W. Koo, J. Jang, D. Kim, Y. Jin, R. Kim, J. Ahn, S. Choi, I. Kim, 2D layer assembly of Pt-ZnO nanoparticles on reduced graphene oxide for flexible NO<sub>2</sub>

- sensors, *Sensor. Actuator. B Chem.* 331 (2021) 129371, <https://doi.org/10.1016/j.snb.2020.129371>.
- [9] J. Lu, D. Li, X. Chen, X. Peng, J. Li, Y. Yang, B. Hong, X. Wang, D. Jin, H. Jin, ZnO/reduced graphene oxide nanocomposite with synergic enhanced gas sensing performance for the effective detection of -NO<sub>2</sub> at room temperature, *J. Nanoparticle Res.* (2022), <https://doi.org/10.1007/s11051-022-05642-w>.
- [10] P. Cao, Y. Cai, D. Pawar, S.T. Navale, C.N. Rao, S. Han, Y. Lu, Down to ppb level NO<sub>2</sub> detection by ZnO/rGO heterojunction based chemiresistive sensors, *Chem. Eng. J.* 401 (2020) 125491, <https://doi.org/10.1016/j.cej.2020.125491>.
- [11] B.W.H. Brattain, J. Bardeen, Surface Properties of Germanium, *Bell Syst. Tech. J.* 32 (1952) 1–41.
- [12] R. Gao, L. Gao, X. Zhang, S. Gao, Y. Xu, X. Cheng, The Controllable Assembly of the Heterojunction Interface of the ZnO @ rGO for Enhancing the Sensing Performance of NO<sub>2</sub> at Room Temperature and Sensing Mechanism, vol. 342, 2021, pp. 1–11.
- [13] Z.U. Abideen, J.H. Kim, A. Mirzaei, H.W. Kim, S.S. Kim, Sensing behavior to ppm-level gases and synergistic sensing mechanism in metal-functionalized rGO-loaded ZnO nanofibers, *Sensor. Actuator. B Chem.* 255 (2018) 1884–1896, <https://doi.org/10.1016/j.snb.2017.08.210>.
- [14] R. Alrammouz, J. Podlecki, P. Abboud, B. Sorli, R. Habchi, A review on flexible gas sensors: from materials to devices, *Sensors Actuators, A Phys.* 284 (2018) 209–231, <https://doi.org/10.1016/j.sna.2018.10.036>.
- [15] P.G. Su, H.C. Shieh, Flexible NO<sub>2</sub> sensors fabricated by layer-by-layer covalent anchoring and in situ reduction of graphene oxide, *Sensor. Actuator. B Chem.* 190 (2014) 865–872, <https://doi.org/10.1016/j.snb.2013.09.078>.
- [16] U. Yaqoob, A.S.M.I. Uddin, G. Chung, *Sensors and Actuators B : Chemical A High-Performance Flexible NO<sub>2</sub> Sensor Based on WO<sub>3</sub> NPs Decorated on MWCNTs and RGO Hybrids on PI/PET Substrates*, vol. 224, 2016, pp. 738–746.
- [17] S. Kim, J. Han, M.A. Kang, W. Song, S. Myung, S.W. Kim, S.S. Lee, J. Lim, K.S. An, Flexible chemical sensors based on hybrid layer consisting of molybdenum disulphide nanosheets and carbon nanotubes, *Carbon N. Y.* 129 (2018) 607–612, <https://doi.org/10.1016/j.carbon.2017.12.065>.
- [18] X.H. Tian, T.Y. Zhou, Y. Meng, Y.M. Zhao, C. Shi, P.X. Hou, L.L. Zhang, C. Liu, H. M. Cheng, A flexible NO<sub>2</sub> gas sensor based on single-wall carbon nanotube films doped with a high level of nitrogen, *Molecules* 27 (2022), <https://doi.org/10.3390/molecules27196523>.
- [19] G. Qu, G. Fan, M. Zhou, X. Rong, T. Li, R. Zhang, J. Sun, D. Chen, Graphene-Modified ZnO nanostructures for low-temperature NO<sub>2</sub> sensing, <https://doi.org/10.1021/acsomega.8b03624>, 2019.
- [20] A. Pathak, S. Samanta, B. Bhargava, S.K. Rajan, J. Bahadur, N.S. Ramgir, M. Kaur, A. Singh, A.K. Debnath, Nanocomposites of ZnO nanostructures and reduced graphene oxide nanosheets for NO<sub>2</sub> gas sensing, *ACS Appl. Nano Mater.* 6 (2023) 7649–7657, <https://doi.org/10.1021/acsnano.3c00117>.
- [21] S.B. Kang, A. Sanger, M.H. Jeong, J.M. Baik, K.J. Choi, Heterogeneous stacking of reduced graphene oxide on ZnO nanowires for NO<sub>2</sub> gas sensors with dramatically improved response and high sensitivity, *Sensor. Actuator. B Chem.* 379 (2023) 133196, <https://doi.org/10.1016/j.snb.2022.133196>.
- [22] D. Li, J. Lu, X. Zhang, D. Jin, H. Jin, Engineering of ZnO/rGO towards NO<sub>2</sub> gas detection: ratio modulated sensing type and heterojunction determined response, *Nanomaterials* 13 (2023), <https://doi.org/10.3390/nano13050917>.
- [23] Y. Zhou, X. Lin, Y. Wang, G. Liu, X. Zhu, Y. Huang, Y. Guo, C. Gao, M. Zhou, Study on gas sensing of reduced graphene oxide/ZnO thin film at room temperature, *Sensor. Actuator. B Chem.* 240 (2017) 870–880, <https://doi.org/10.1016/j.snb.2016.09.064>.
- [24] A.D. Ugale, G.G. Umarji, S.H. Jung, N.G. Deshpande, W. Lee, H.K. Cho, J.B. Yoo, ZnO decorated flexible and strong graphene fibers for sensing NO<sub>2</sub> and H<sub>2</sub>S at room temperature, *Sensor. Actuator. B Chem.* 308 (2020) 127690, <https://doi.org/10.1016/j.snb.2020.127690>.
- [25] Z. Chen, H. Guo, F. Zhang, X. Li, J. Yu, X. Chen, Porous ZnO/rGO nanosheet-based NO<sub>2</sub> gas sensor with high sensitivity and ppb-level detection limit at room temperature, *Adv. Mater. Interfac.* 8 (2021) 1–11, <https://doi.org/10.1002/admi.202101511>.
- [26] H. Gao, Y. Ma, P. Song, J. Leng, Q. Wang, Gas sensor based on rGO/ZnO aerogel for efficient detection of NO<sub>2</sub> at room temperature, *J. Mater. Sci. Mater. Electron.* 32 (2021) 10058–10069, <https://doi.org/10.1007/s10854-021-05664-5>.
- [27] T.M. Milão, J.F.A. Oliveira, V.D. Araújo, M.I.B. Bernardi, ZnO.97Mn.03O (M = Co, Fe, and V) pigments: thermal, structural, and optical characterization, *J. Therm. Anal. Calorim.* 103 (2011) 873–877, <https://doi.org/10.1007/s10973-010-1107-z>.
- [28] M.A. Franco, P.P. Conti, R.S. Andre, D.S. Correa, A review on chemiresistive ZnO gas sensors, *Sensors and Actuators Reports* 4 (2022) 100100, <https://doi.org/10.1016/j.snr.2022.100100>.
- [29] V.S. Bhati, M. Kumar, R. Banerjee, Gas sensing performance of 2D nanomaterials/metal oxide nanocomposites: a review, *J. Mater. Chem. C* 9 (2021) 8776–8808, <https://doi.org/10.1039/d1tc01857d>.
- [30] R. Beams, L. Gustavo Caçado, L. Novotny, Raman characterization of defects and dopants in graphene, *J. Phys. Condens. Matter* 27 (2015), <https://doi.org/10.1088/0953-8984/27/8/083002>.
- [31] A.C. Ferrari, D.M. Basko, Raman spectroscopy as a versatile tool for studying the properties of graphene, *Nat. Nanotechnol.* 8 (2013) 235–246, <https://doi.org/10.1038/nnano.2013.46>.
- [32] R. Arul, R.N. Oosterbeek, J. Robertson, G. Xu, J. Jin, M.C. Simpson, The mechanism of direct laser writing of graphene features into graphene oxide films involves photoreduction and thermally assisted structural rearrangement, *Carbon N. Y.* 99 (2016) 423–431, <https://doi.org/10.1016/j.carbon.2015.12.038>.
- [33] A. Jorio, E.H.M. Ferreira, F. Stavale, C.A. Achete, R.B. Capaz, M.V.O. Moutinho, A. Lombardo, T.S. Kulmala, A.C. Ferrari, Quantifying defects in graphene via Raman spectroscopy at different excitation energies, 3190–3196, <https://doi.org/10.1021/nl201432g>, 2011.
- [34] D.S. Sutar, P.K. Narayanam, G. Singh, V.D. Botcha, S.S. Talwar, R.S. Srinivasa, S. S. Major, Spectroscopic studies of large sheets of graphene oxide and reduced graphene oxide monolayers prepared, *Langmuir – Blodgett technique* 520 (2012) 5991–5996, <https://doi.org/10.1016/j.tsf.2012.05.018>.
- [35] S. Claramunt, A. Varea, D. López-Díaz, M.M. Velázquez, A. Cornet, A. Cirera, The importance of interbands on the interpretation of the Raman spectrum of graphene oxide, *J. Phys. Chem. C* 119 (2015) 10123–10129, <https://doi.org/10.1021/acs.jpcc.5b01590>.
- [36] J. Hu, G. Kong, Y. Zhu, C. Che, Ultrafast room-temperature reduction of graphene oxide by sodium borohydride, sodium molybdate and hydrochloric acid, *Chin. Chem. Lett.* 32 (2021) 543–547, <https://doi.org/10.1016/j.ccl.2020.03.045>.
- [37] D. López-Díaz, J.A. Delgado-Notario, V. Clericò, E. Diez, M.D. Merchán, M. M. Velázquez, Towards understanding the Raman spectrum of graphene oxide: the effect of the chemical composition, *Coatings* 10 (2020), <https://doi.org/10.3390/COATINGS10060524>.
- [38] A. Bhaumik, J. Narayan, Conversion of p to n-type reduced graphene oxide by laser annealing at room temperature and pressure, *J. Appl. Phys.* 121 (2017), <https://doi.org/10.1063/1.4979211>.
- [39] R.L. de S. e Silva, A. Franco Jr., Raman spectroscopy study of structural disorder degree of ZnO ceramics, *Mater. Sci. Semicond. Process.* 119 (2020) 105227, <https://doi.org/10.1016/j.mssp.2020.105227>.
- [40] F.J. Sonia, H. Kalita, M. Aslam, A. Mukhopadhyay, Correlations between preparation methods, structural features and electrochemical Li-storage behavior of reduced graphene oxide, *Nanoscale* 9 (2017) 11303–11317, <https://doi.org/10.1039/C7NR03348F>.
- [41] I.V. Korolkov, A.B. Yeszhanov, M.V. Zdorovets, Y.G. Gorin, O. Güven, S. S. Dosmagambetova, N.A. Khlebnikov, K.V. Serkov, M.V. Krasnopyorova, O. S. Milts, D.A. Zheltov, Modification of PET ion track membranes for membrane distillation of low-level liquid radioactive wastes and salt solutions, *Sep. Purif. Technol.* 227 (2019) 115694, <https://doi.org/10.1016/j.seppur.2019.115694>.
- [42] H.-J. Lee, J.S. Kim, K.Y. Lee, K.H. Park, J.-S. Bae, M. Mubarak, H. Lee, Elucidation of an intrinsic parameter for evaluating the electrical quality of graphene flakes, *Sci. Rep.* 9 (2019) 557, <https://doi.org/10.1038/s41598-018-37010-x>.
- [43] J. Dupin, D. Gonbeau, A. Levasseur, P. Cedex, T. Cedex, *Systematic XPS studies of metal oxides. Hydroxides and Peroxides*, 2000, pp. 1319–1324.
- [44] N. Kumar, A.K. Srivastava, H.S. Patel, B.K. Gupta, G. Das Varma, Facile synthesis of EuO-reduced graphene oxide nanocomposites for NO<sub>2</sub> gas sensing applications, *Eur. J. Inorg. Chem.* 2015 (2015) 1912–1923, <https://doi.org/10.1002/ejic.201403172>.
- [45] P.S. Behera, S. Bhattacharyya, Effect of different alumina sources on phase formation and densification of single-phase mullite ceramic – Reference clay alumina system, *Mater. Today Commun.* 26 (2021) 101818, <https://doi.org/10.1016/j.mtcomm.2020.101818>.
- [46] M.A. Alouani, J. Casanova-Cháfer, F. Güell, E. Peña-Martín, S. Ruiz-Martínez-Alcocer, S. de Bernardi-Martín, A. García-Gómez, X. Vilanova, E. Llobet, ZnO-loaded graphene for NO<sub>2</sub> gas sensing, *Sensors* 23 (2023) 6055, <https://doi.org/10.3390/s23136055>.
- [47] H. Park, W. Kim, S.W. Lee, J. Park, G. Lee, D.S. Yoon, W. Lee, J. Park, Flexible and disposable paper-based gas sensor using reduced graphene oxide/chitosan composite, *J. Mater. Sci. Technol.* 101 (2022) 165–172, <https://doi.org/10.1016/j.jmst.2021.06.018>.
- [48] D. Bin Moon, A. Bag, H.B. Lee, M. Meesepong, D.H. Lee, N.E. Lee, A stretchable, room-temperature operable, chemiresistive gas sensor using nanohybrids of reduced graphene oxide and zinc oxide nanorods, *Sensor. Actuator. B Chem.* 345 (2021) 130373, <https://doi.org/10.1016/j.snb.2021.130373>.
- [49] X. Chen, D. Li, S. Liang, X. Li, S. Zhan, M. Liu, Novel Flexible Room Temperature NO<sub>2</sub> Gas Sensor Based on Polypyrrole Coated SnO<sub>2</sub> Nanoparticles, vol. 1 (n.d.) 2–5.
- [50] B. Cho, A.R. Kim, D.J. Kim, H.S. Chung, S.Y. Choi, J.D. Kwon, S.W. Park, Y. Kim, B. H. Lee, K.H. Lee, D.H. Kim, J. Nam, M.G. Hahm, Two-dimensional atomic-layered alloy junctions for high-performance wearable chemical sensor, *ACS Appl. Mater. Interfaces* 8 (2016) 19635–19642, <https://doi.org/10.1021/acsami.6b05943>.
- [51] R. Paul, B. Das, R. Ghosh, Novel approaches towards design of metal oxide based hetero-structures for room temperature gas sensor and its sensing mechanism. A recent progress, *J. Alloys Compd.* 941 (2023) 168943, <https://doi.org/10.1016/j.jallcom.2023.168943>.
- [52] J. Won, A. Kim, Absolute work function measurement by using photoelectron spectroscopy, *Curr. Appl. Phys.* 31 (2021) 52–59, <https://doi.org/10.1016/j.cap.2021.07.018>.
- [53] A.P. Baddori, Identifying the secondary electron cutoff in ultraviolet photoemission spectra for work function measurements of non - ideal surfaces, *Sci. Rep.* (2023) 1–8, <https://doi.org/10.1038/s41598-023-40187-5>.
- [54] T. Vu Anh, T.A.T. Pham, V.H. Mac, T.H. Nguyen, Facile controlling of the physical properties of zinc oxide and its application to enhanced Photocatalysis, *J. Anal. Methods Chem.* 2021 (2021) 1–12, <https://doi.org/10.1155/2021/5533734>.
- [55] S. Roso, C. Bittencourt, P. Umek, O. González, F. Güell, A. Urakawa, E. Llobet, Synthesis of single crystalline In<sub>2</sub>O<sub>3</sub> octahedra for the selective detection of NO<sub>2</sub>

- and H<sub>2</sub> at trace levels, *J. Mater. Chem. C* 4 (2016) 9418–9427, <https://doi.org/10.1039/c6tc03218d>.
- [56] R.G. Pavelko, H. Daly, C. Hardacre, A.A. Vasiliev, E. Llobet, Interaction of water, hydrogen and their mixtures with SnO<sub>2</sub> based materials: the role of surface hydroxyl groups in detection mechanisms, *Phys. Chem. Chem. Phys.* 12 (2010) 2639–2647, <https://doi.org/10.1039/b921665k>.
- [57] S. Roso, D. Degler, E. Llobet, N. Barsan, A. Urakawa, Temperature-dependent NO<sub>2</sub> sensing mechanisms over indium oxide, *ACS Sens.* 2 (2017) 1272–1277, <https://doi.org/10.1021/acssensors.7b00504>.